

Ultra-narrow linewidth hybrid integrated semiconductor laser

Youwen Fan¹, Albert van Rees¹, Peter J.M. van der Slot^{1,*}, Jesse Mak¹, Ruud M. Oldenbeuving², Marcel Hoekman², Dimitri Geskus², Chris G.H. Roeloffzen², and Klaus-J. Boller¹

¹Laser Physics and Nonlinear Optics, Mesa+ Institute for Nanotechnology, Department for Science and Technology, University of Twente, Enschede, The Netherlands

²LioniX International BV, Enschede, The Netherlands

*Corresponding author: p.j.m.vanderslot@utwente.nl

May 25, 2022

Abstract

We demonstrate a hybrid integrated and widely tunable diode laser with an intrinsic linewidth as narrow as 40 Hz, achieved with a single roundtrip through a low-loss feedback circuit that extends the cavity length to 0.5 meter on a chip. Employing solely dielectrics for single-roundtrip, single-mode resolved feedback filtering enables linewidth narrowing with increasing laser power, without limitations through nonlinear loss. We achieve single-frequency oscillation with up to 23 mW fiber coupled output power, 70-nm wide spectral coverage in the 1.55 μ m wavelength range with 3 mW output, and obtain more than 60 dB side mode suppression. Such properties and options for further linewidth narrowing render the approach of high interest for direct integration in photonic circuits serving microwave photonics, coherent communications, sensing and metrology with highest resolution.

1 Introduction

Semiconductor lasers with narrow linewidth and wide tunability are of central interest in photonic applications where controlling the optical phase is es-

sential, for instance for microwave photonics [1], optical beamforming networks [2], coherent optical communications [3], light detection and ranging (LIDAR) [4], optical sensing [5], or precision metrology and timing, including GPS systems [6, 7, 8]. Of particular interest are narrow linewidth semiconductor lasers for pumping Raman and Brillouin lasers [9, 10, 11], integration into functional photonic circuits, to serve as light engines, such as for electrically driven and fully integrated Kerr frequency combs [12, 13].

A measure for a laser’s ultimate phase stability is the intrinsic linewidth (Schawlow-Townes limit), which can only be narrowed via increasing the photon lifetime of the laser cavity, or via increasing the laser power [14, 15]. However, in monolithic diode lasers both is problematic due to linear and nonlinear loss. The intrinsic waveguiding loss in semiconductor amplifiers is high, which limits the photon lifetime. The spectral filtering circuitry required for single-frequency oscillation causes additional loss, at high laser power also nonlinear loss occurs, while efficient output coupling decreases the lifetime further. This leads to large intrinsic linewidths typically in the range of a MHz [16].

Many orders of magnitude smaller linewidths have been achieved with hybrid and heterogeneously in-

tegrated diode lasers, ultimately reaching into the sub-kHz-range. In all these approaches the cavity is extended with additional waveguide circuitry fabricated from a different material platform selected for low loss. On the other hand, hybrid and heterogeneous integration add further loss due to imperfect optical coupling between distinct platforms and materials.

For extending the cavity length and maintaining single longitudinal mode oscillation, spectral filtering has mostly been based on microring resonators employing Si waveguides [17, 18, 19, 20], SiON [21], SiO₂ [22] and Si₃N₄ [23, 24, 25], thereby reducing the linewidth from hundreds of kilohertz [18, 25] to 220 Hz [20]. Silicon waveguides bear the advantage of heterogeneous integration [26, 27]. However, beyond certain intra-cavity intensities and laser powers, using silicon limits the lowest achievable linewidth through nonlinear loss [28, 26], specifically, due to two-photon absorption across the relatively small bandgap of silicon [29]. Avoiding high intensities is difficult when having to select a single longitudinal mode within the wide semiconductor gain spectrum, because high-finesse filtering for strong side mode suppression is associated with resonantly enhanced power. Relying on external amplification and operating the diode laser at low power is not a viable route, because the linewidth increases inversely with lowering the laser output [14].

Here we present a hybrid integrated semiconductor laser with an intrinsic linewidth as low as 40 Hz. This is achieved by realizing a laser cavity of long photon lifetime, in spite of almost 100% roundtrip loss, and in spite of high intracavity intensity. A scheme of the laser is displayed in Fig. 1 (a), comprising an InP semiconductor amplifier and a dielectric, low-loss silicon nitride waveguide feedback circuit for cavity length extension. Narrow linewidth is achieved with three basic considerations. The first is providing a long photon lifetime already in a single roundtrip through a low-loss and long extension circuit. This decouples the laser cavity photon lifetime from intrinsically high loss in the remaining parts of the cavity, specifically, in the semiconductor amplifier, but also from loss at mode coupling between waveguide platforms, and due to strong output coupling

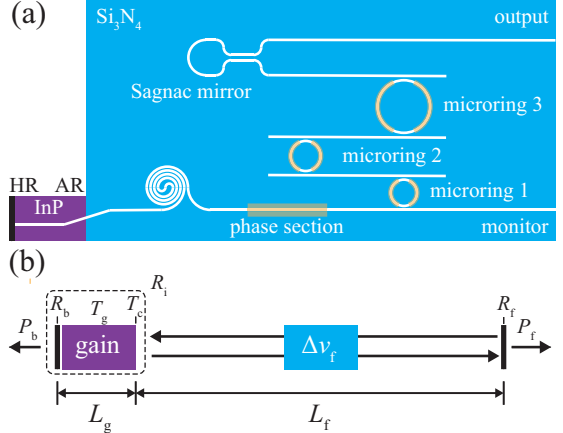


Figure 1: (a) Schematic view of the hybrid laser comprising an InP gain section and a Si₃N₄ feedback circuit that extends the cavity length by a large factor with regard to the solitary semiconductor chip. (b) Extending the laser cavity with a long and low-loss feedback arm ($L_f \gg L_g$ and $R_f \gg R_i$) increases the photon lifetime and narrows the laser linewidth, even in the presence of high intrinsic roundtrip loss (low R_i) in the remaining part of the cavity (dashed region). T_g : transmission of gain section, T_c : mode coupling efficiency at the interface, R_b : back facet reflectance, R_f : overall feedback reflectance from extended cavity arm, $\Delta\nu_f$: double-pass bandwidth of spectral filter used to impose single-frequency oscillation.

for increased power efficiency. Second, we exploit low propagation loss in the cavity extension to implement single-mode resolved spectral filtering already in a single roundtrip through the extension. This imposes single-mode oscillation with high side mode suppression, which enables adjusting for stable laser operation at lowest linewidth without spectral mode hops. Third, to prevent that nonlinear loss does not compromise the photon lifetime, we use a wide-bandgap dielectric waveguide platform for laser cavity extension and restrict high-finesse spectral filtering solely to the dielectric part of the cavity. Thereby the laser linewidth can be decreased inversely with increasing the laser output.

2 Conditions for narrow linewidth

To illustrate the key ingredients in our approach we recall the main conditions to induce narrow linewidth in extended cavity single-mode diode lasers [30, 31, 32, 33, 34]. The first condition is a long photon lifetime because this increases the phase memory time of the laser resonator. If the total roundtrip loss can be reduced to below a few percent, the photon lifetime can be extended via multiple roundtrips in a short resonator [26]. In this case, due to the large free spectral range of short resonators, lower-finesse intracavity spectral filtering is sufficient for achieving single-mode oscillation. However, this approach is usually hard to realize due to intrinsically high passive roundtrip loss in semiconductor lasers.

Our approach provides a long photon lifetime in spite of high roundtrip loss, by extending the laser cavity with a long feedback arm as displayed in Fig. 1 (b). Extending the cavity length can reduce the laser linewidth almost inversely quadratic with the feedback length, L_f . However, this requires that the overall loss in the feedback arm, due to waveguide, filtering and outcoupling loss, remains much smaller than the intrinsic loss in the remaining part of the laser cavity roundtrip. In terms of roundtrip reflectivities this can be expressed as $R_f \gg R_i$, where R_f is the effective reflectance of the feedback and where $R_i = R_b T_g^2 T_c^2$ lumps all loss of the remaining roundtrip into an intrinsic reflectance. Here, $T_g = e^{(-\alpha_i L_g)} < 1$ is the power transmission in a single pass through the gain section with α_i the intrinsic passive loss constant of the gain waveguide and L_g the length of the amplifier. $T_c < 1$ specifies mode coupling loss per transmission through the interface between platforms, and $R_b < 1$ describes loss due to an imperfectly reflecting amplifier backfacet. To illustrate that sufficiently high feedback reflectivity yields linewidth narrowing via cavity length extension, we recall how the intrinsic linewidth scales with cavity loss and cavity length [35]

$$\Delta\nu_{ST} = C \frac{\gamma_{tot}\gamma_m F_P}{(P_0 K) F^2}. \quad (1)$$

Here, $\gamma_{tot} = 1/(2L_g) \ln(\frac{1}{R_i R_f})$ is the spatially distributed roundtrip loss coefficient, $\gamma_m = 1/(2L_g) \ln(\frac{1}{R_b R_f})$ the distributed mirror loss coefficient, P_0 the output power at a particular output port, and $K > 1$ a weight factor accounting for additional power emitted at other ports. $F_P > 1$ is the longitudinal Petermann factor increasing the linewidth, in case that reflective feedback (R_b and R_f) becomes very small [32, 31]. Linewidth narrowing via cavity length extension is expressed by the factor $F = (n_f L_f)/(n_g L_g)$, assuming that $L_f \gg L_g$, and where n is the effective group index in the respective waveguides. The overall factor C includes the spontaneous emission factor, photon energy and amplifier group velocity. Linewidth enhancement via gain-index coupling [36] is not included in C due to compensation by F with frequency-loss coupling in a long, frequency selective feedback arm [37, 38, 34].

To show that in Eq. 1 the linewidth narrows almost inversely quadratic with length, as long as the external feedback is stronger than intrinsic feedback, we insert typical diode amplifier parameters as $\alpha_i = 1600 \text{ m}^{-1}$, $L_g = 1 \text{ mm}$, and $R_b = 90\%$ [35]. Even with assuming very good coupling ($T_c=90\%$), the typical intrinsic feedback turns out to be at the lower-percent level, here $R_i \approx 3\%$. The consequence is that the coefficient for the total roundtrip loss, γ_{tot} , is mainly given by R_i , and thus is largely independent of R_f , as long as $R_f \gg 3\%$. For instance, if changing R_f by a factor of two from 50 to 25%, such as might occur by doubling the feedback length, γ_{tot} increases only slightly, from 4.2 to 4.9 (in units of $1/[2L_g]$). On the other hand, doubling the feedback length increases F^2 by a factor of four. The combined contribution to linewidth narrowing is then close to a factor of 3.5. Other factors in Eq. 1 approximately compensate each other or do not change much at all. As long as the laser operates well above threshold, increasing the mirror loss coefficient γ_m is compensated by an increasing power weight factor K . The Petermann factor remains at values close to unity.

Although a thorough theoretical exploration of all interdependences is not available at this moment, the given example illustrates that in spite of the typically high intrinsic loss, here 97% ($R_i \approx 3\%$), cavity length

extension yields strong linewidth narrowing, as long as the external feedback reflectivity remains noticeably higher than the intrinsic feedback. The weak dependence of the total roundtrip loss, γ_{tot} upon cavity extension with efficient feedback is the key to ultra-narrow linewidth.

The second condition is a sufficiently high spectral resolution of the feedback filter. This is required for coping with the coupling of the refractive index and gain in semiconductor amplifiers as quantified by Henry's linewidth enhancement factor. The coupling enhances the linewidth because gain fluctuations, for instance through spontaneous emission, cause additional index fluctuations that increase the phase noise. To counteract the effect with an extended cavity, the feedback arm has to be strongly frequency selective to introduce frequency-loss coupling by operating the laser at the low-frequency side of the feedback filter transmission. Enabling stable laser operation by fine tuning for lowest linewidth without spectral mode hops requires single-mode resolved spectral filtering in the feedback arm. Single-mode filtering is obtained if the FWHM resolution of the filter, $\Delta\nu_f$, is narrower than the laser cavity mode spacing.

The third condition for narrow linewidth is operating the laser maximally high above threshold. This reduces the relative rate of randomly phased spontaneous emission as compared to phase-preserving stimulated emission. At a given roundtrip loss, high-above-threshold operation can only be achieved by increasing the pump power. In the experiments, we increase the laser power for linewidth narrowing. To maintain single-mode oscillation with high-finesse spectral filtering, we use a dielectric waveguide platform for extending the cavity length, where spectral filtering is implemented only with dielectric materials. This choice ensures that high intracavity intensity, occurring at high laser power due to filter-induced enhancement, is only present in the dielectric part of the laser. There, nonlinear loss can be safely neglected due to the wide bandgap of dielectric materials.

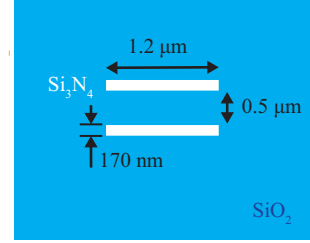


Figure 2: Schematic view of the cross section of the double stripe Si_3N_4 waveguide used in the photonic feedback circuit for the hybrid laser.

3 Laser design

Figure 1 shows the schematic design of the hybrid laser, comprising an InP semiconductor optical amplifier (gain section) and an extended cavity made of a long Si_3N_4 low-loss dielectric waveguide circuit that provides frequency selective feedback to the amplifier.

The InP semiconductor amplifier (COVEGA, SAF 1126) for generation of light at around $1.55 \mu\text{m}$ wavelength has a length of $1000 \mu\text{m}$ and specified typical output power of 60 mW based on amplification in multiple quantum wells. The back facet is high-reflection coated ($R=90\%$) to provide double-pass amplification. In order to suppress back-reflection into the amplifier, the front facet is anti-reflection coated to a specified reflectivity of 10^{-4} for an external index of 1.5, which is close to the effective refractive index of the tapered input end of the Si_3N_4 waveguide circuit (1.584). The semiconductor waveguide is tilted by 6° , to further reduce back-reflection. Derived from the far-field specifications, the mode field diameter at the exit facet is $4.4 \mu\text{m}$ in the horizontal and $1.3 \mu\text{m}$ in the vertical direction. The amplifier is integrated with the Si_3N_4 circuit via alignment for maximizing the amount of amplified spontaneous emission (ASE) entering the Si_3N_4 circuit, followed by bonding with an adhesive. The integrated laser is mounted on a thermoelectric cooler and kept at 25°C . The electrical connects are wire bonded to a fan-out electronic circuit board. For driving the amplifier with a low-noise current, we use a battery-driven power supply (ILX Lightwave, LDX3620).

A long optical path length for linewidth narrowing, and sharp spectral filtering for single-mode oscillation, is provided with a Si_3N_4 circuit optimized for low-loss and high frequency selectivity. In this platform [39] the core cross section can be adjusted to obtain a proper combination of tight guiding and low loss. We select a symmetric double-stripe geometry, see Fig. 2, that comprises two Si_3N_4 cores ($1.2 \mu\text{m} \times 170 \text{ nm}$) separated by 500 nm embedded in a SiO_2 cladding. This cross section yields single-spatial mode propagation for the TE polarization and an effective group index of 1.715. The propagation loss is smaller than 0.1 dB/cm , concluded from light scattering measurements with an IR camera. The chosen cross section and the high index contrast between core and cladding ($\Delta n \approx 0.53$) provides tight guiding, making radiative loss (bending loss) negligible also for waveguides with tight bending radii, as small as $100 \mu\text{m}$. This enables to employ small-radius, low-loss microring resonators for Vernier-filtering with a wide free spectral range (FSR) comparable to the gain bandwidth [23]. Tight guiding in combination with low loss enables to realize significant on-chip optical path lengths. For instance, with a loss coefficient of 0.1 dB/cm and allowing that the returning power drops to a fraction of $R_f = 1/e$, enables to extend the laser cavity optical roundtrip length to about 75 cm . This corresponds to extending the photon lifetime to around two nanoseconds. The selected waveguide cross section is also suitable for low-loss adiabatic tapering. With two-dimensional tapering, the calculated maximum power coupling to the mode field of the gain section is in the range of $T_c = 90$ to 93% [40], and the coupling to the $10.5 \pm 0.8 \mu\text{m}$ diameter mode of single-mode output fibers (Fujikura 1550PM) can be as high as 98% .

At this point we recall that we do not aim on low loss per entire roundtrip through the hybrid cavity. Instead we maximize only the optical length and thus the photon travel time in the dielectric feedback arm of the laser cavity, while keeping the loss in the feedback arm much lower than the intrinsic loss in the remaining part of the laser cavity roundtrip. With the circuit design realized here, the feedback arm provides a high peak reflectivity of $R_f = 51\%$. In contrast, the loss in the remaining parts of the laser

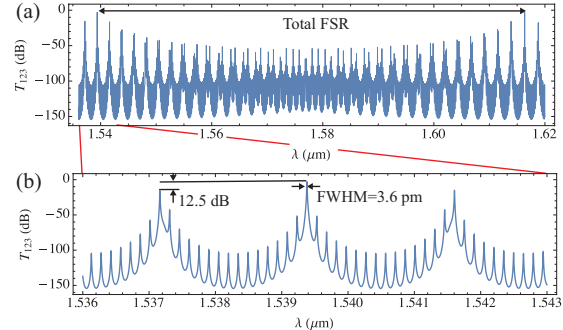


Figure 3: Power transmission T_{123} of the Si_3N_4 feed-back arm containing three cascaded rings with radii $R_1 = 99 \mu\text{m}$, $R_2 = 102 \mu\text{m}$ and $R_3 = 1485 \mu\text{m}$ across a range corresponding to the gain bandwidth (a) and across a small range near the maximum of the gain at $1.54 \mu\text{m}$ (b). The peak transmission amounts to 51% as calculated with an effective group index of $n_g = 1.715$, the Sagnac mirror reflectance set to 90%, and a propagation loss of 0.1 dB/cm .

cavity is much higher, *i.e.*, $R_i \approx 3\%$. The latter is calculated from double-passing 80% loss in the amplifier, 10% loss at the amplifier back facet, and double-passing 10% loss at the InP- Si_3N_4 interface. The loss estimates show that the laser would operate in the strong feedback regime, where $R_f \gg R_i$, such that a long roundtrip length in the feedback circuit should enable significant linewidth narrowing.

In order to induce single frequency oscillation across the 70 nm (8 THz) wide gain bandwidth in spite of an expected, dense mode spacing of a long laser cavity, we use three cascaded microring resonators in add-drop configuration, all with a power coupling of 10% to their bus waveguides. Two short resonators with a small difference in radius are used in Vernier configuration for coarse frequency selection ($R = 99$ and $102 \mu\text{m}$, average FSR 278 GHz, finesse 28, quality factor $Q \approx 2,000$). The third microring resonator provides fine spectral filtering ($R_3 = 1485 \mu\text{m}$, FSR 18.6 GHz, finesse 28, $Q \approx 290,000$). Behind the resonators the extended cavity is closed with a Sagnac loop mirror of adjustable reflectivity via a balanced Mach-Zehnder interferom-

eter. Taking into account that all resonators are double-passed in the silicon nitride feedback circuit and assuming 0.1 dB/cm propagation loss, we calculate a FWHM of the spectral filter's transmission peak of 450 MHz (3.6 pm).

For spectrally aligned and resonant microring resonators, we calculate a laser cavity optical roundtrip length of $2L = 0.49\text{ m}$ which, via $\text{FSR} = c/(2L)$, corresponds to a free spectral range of 607 MHz. The length is calculated with double-passing the optical length of the three resonators multiplied each with the approximate number of nine round trips at resonance [41], a 33 mm long waveguide spiral for further cavity length extension, the length of the amplifier, and various smaller sections of bus waveguides including the loop mirror. We note that the cavity mode spacing varies noticeably with the light frequency, which is mainly due to strong dispersion in transmission through the long microring resonator. For light at transmission resonance of the long resonator, this places the two closest cavity modes at 965 MHz distance. For light in the midpoint wing of the transmission resonance, the closest both done cavity mode is located at 750 MHz. In comparison, the 450-MHz bandwidth of the feedback filtering is smaller, *i.e.*, the condition of single-mode resolved filtering is fulfilled.

The calculated double-pass filter spectrum obtained with the three-ring circuit across a range corresponding to the gain bandwidth is shown in Fig. 3(a) and across a small range around the resonant wavelength of $1.5359\text{ }\mu\text{m}$ in Fig. 3(b). For a Sagnac mirror reflectivity of 90%, as used for spectral recordings, we calculate a high feedback of $R_f = 51\%$, which is due to low loss in the Si_3N_4 waveguides. The feedback at the next-highest side resonance of the long resonator is lower by -12.5 dB. For setting the highest transmission peak to any laser cavity mode within the laser gain, the resonators are equipped with thin-film thermo-electric phase shifters with a $0 - 2\pi$ range. With the described spectral filtering and due to the dominance of homogeneous gain broadening in the quantum well amplifier, it is expected that single-mode oscillation with high side mode suppression ratio is possible at any wavelength within the gain bandwidth.

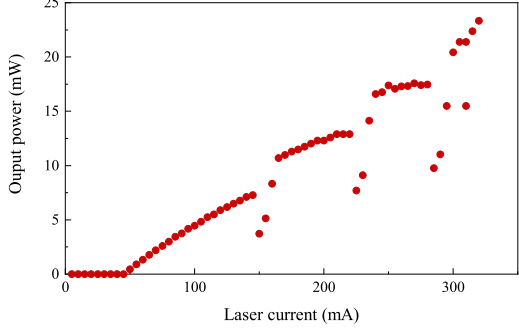


Figure 4: Laser output power as measured with increasing pump current, yielding a maximum output of 23 mW. The discontinuities indicate spectral mode hops.

4 Results

Figure 4 shows the measured fiber-coupled output power behind the Sagnac loop mirror vs pump current. For achieving high output, the Sagnac mirror was set to a high transmission of about 80%, and the laser wavelength was set to the center of the gain spectrum via the phase shifter of the first microring resonator. The pump current is stepwise varied and fine-tuned, in order to maintain single-mode operation. The laser shows a threshold pump current of about 42 mA and a maximum output power of 23 mW is achieved at a pump current of 320 mA. This is approximately half of the specified maximum power of the amplifier of 50 mW. The discontinuities in the output power vs. pump current correspond to spectral mode hops. The reason is that increasing the pump current also changes the refractive index in the amplifier, which tunes the laser cavity length with regard to the transmission spectrum of the feedback filter.

To discuss the presence of nonlinear loss, we estimate the maximum intracavity intensity that occurs at the maximum output power. Assuming a Sagnac mirror transmission of 10%, we calculate a power of approximately 4 W in the long resonator (2 W in each direction). Using a mode area of $1.6 \times 1.7\text{ }\mu\text{m}^2$ the according intensity is high, of the or-

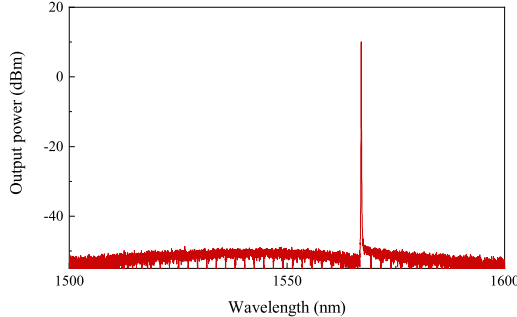


Figure 5: Output power spectrum recorded with a resolution of 50 pm (6 GHz).

der of 0.15 GW/cm^2 . However, loss from two-photon absorption can safely be neglected [42] due to the wide bandgap of Si_3N_4 . For comparison, in a silicon waveguide the same power and a typical mode field area of $0.5 \times 0.5 \mu\text{m}^2$ would cause significant two-photon absorption, *i.e.*, of the order of 5 dB/cm [29]. This would make it difficult to implement sharp spectral filtering, to realize long, resonator-enhanced feedback lengths, and to narrow the linewidth via the laser power.

To verify that the laser oscillates at a single wavelength, the laser output spectrum is measured at the fiber-coupled output from the through port of the first small resonator (monitor port in Fig. 1). There it would be possible to observe also light that is not resonant with the microring resonators. The spectrum is measured using an optical spectrum analyzer (OSA: ANDO AQ6317) after tuning the small resonators for single-mode oscillation. All spectral measurements are performed behind an optical isolator and using tilted fiber connections to avoid feedback into the laser. Fig. 5 shows a typical laser output spectrum, obtained at a driving current of 200 mA and recorded across a spectral range from 1500 nm to 1600 nm, with a resolution of 50 pm (6 GHz).

The presence of a single peak with a side mode suppression ratio of 60 dB suggests single-mode oscillation. Such spectra can be observed typically over time intervals between ten minutes and one hour without any frequency stabilization. The spectrum shows a slightly asymmetric ASE background near

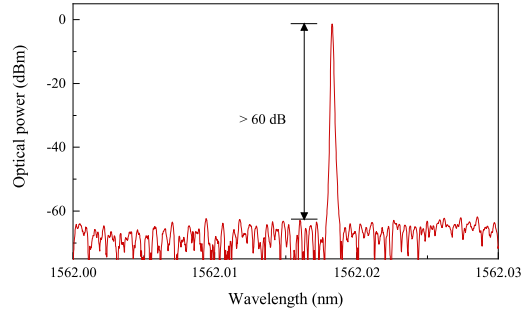


Figure 6: Power spectrum recorded across a range of 30 pm with 0.1 pm resolution ((3.7 GHz and 12 MHz, respectively)).

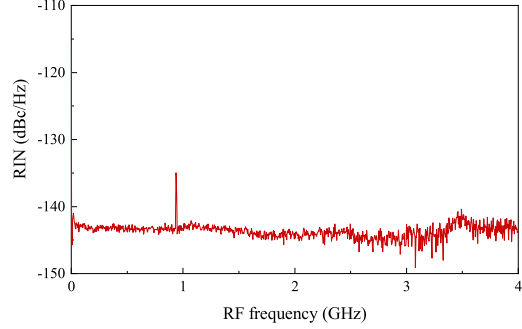


Figure 7: Power spectrum of the relative intensity noise (RIN). The spectrum is flat except for a small peak around 950 MHz.

the main longitudinal mode, which may be addressed to asymmetric nonlinear gain saturation [43]. However, it should be noticed that the emission spectrum is not fully resolved compared to the calculated mode spacing.

To obtain a higher resolution than the mode spacing, the laser spectrum was recorded with a second spectrum analyzer based on stimulated Brillouin scattering (Aragon Photonics, BOSA400). Figure 6 shows the power spectrum recorded with the maximum resolution of 0.1 pm (12 MHz) across a 30 pm (3.7 GHz) wide interval around the oscillating mode. This range spans four to five mode spacings, such that possibly oscillating side modes would have become detectable. The measured spectrum confirms clean

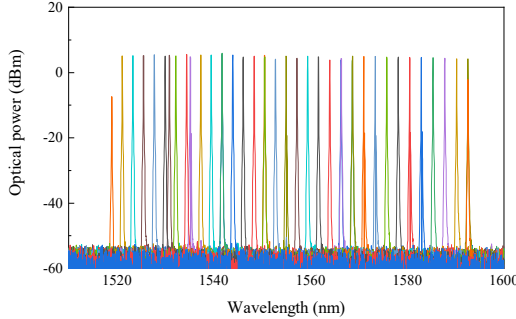


Figure 8: Superimposed output spectra recorded by tuning the laser wavelength in steps of 2 nm across a range of > 70 nm.

single-mode oscillation, with even a slightly higher side mode suppression of about 62 dB.

For further characterization we measure relative intensity noise (RIN) with a fast photodiode and RF spectrum analyzer (10 kHz resolution and 100 kHz video bandwidth). The RIN spectrum in Fig. 7 displays flat, broadband and low intensity noise around -142 dBc/Hz. Single narrowband features, here at 940 MHz, are likely due to RF pickup, as not all spectra display these.

To explore the overall spectral coverage of single-mode oscillation, the laser was manually tuned via the phase shifters on top of the microring resonators using a maximum heater power of 270 mW per heater. Figure 8 shows an example of superimposed laser spectra, with the laser tuned to 35 different wavelengths. For coarse wavelength tuning, the heater current of one of the small microresonators is increased. This gives rise to discrete wavelength changes at a stepsize of about 2 nm, which corresponds to the FSR of the other small resonator. After the wavelength is set to a desired value, also the heating current of the other small resonator is adjusted for maximum laser output, to improve the spectral alignment of all resonators. The approximately flat tuning envelope is obtained by adjusting the Sagnac mirror feedback with wavelength tuning, at a current of 200 mA. We obtain a spectral coverage of 74 nm and at least 3 mW of output power. This compares well with the current record for monolithic, hetero-

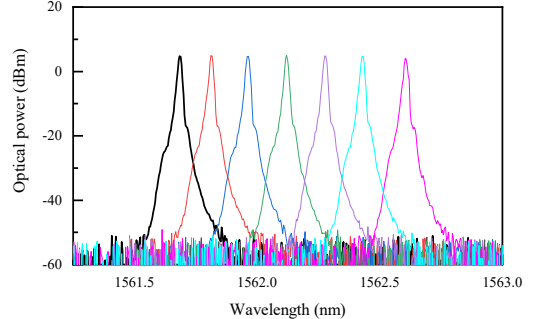


Figure 9: Superimposed spectra when fine tuning the laser in steps of 0.15 nm.

geneously and hybrid integrated lasers [44, 25, 20]. Fine-tuning shown in steps of the FSR of the long resonator is shown in Fig. 9. This was achieved via tuning the small resonators and loop mirror without heating the long resonator.

The intrinsic linewidth of the laser is measured using two independent setups based on delayed self-heterodyne detection [45, 46]. The first uses a Mach-Zehnder interferometer with 5.4 m optical arm length difference, a 40-MHz acousto-optic modulator, and two photodiodes for balanced detection. The beat signal is recorded versus time and analyzed with a computer to obtain the power spectral density of frequency noise (PSD). Free-running lasers, as investigated here, typically display increased technical noise at low frequencies whereas, at high noise frequencies, the PSD level levels off to the intrinsic laser linewidth. The second uses an arm length difference of 20 km and an 80-MHz modulator. The power spectrum of the beat signal is recorded with an RF spectrum analyzer. The intrinsic linewidth is retrieved with Lorentzian fits to the linewidths where the Lorentzian shape is minimally obstructed, *i.e.*, avoiding the low-frequency noise regime near the line center, as well as the range close to the electronic noise floor. Linewidth measurements are carried at various different pump currents at a wavelength near the center of the gain spectrum.

Figure 10 shows the PSD measured at a pump current of 255 mA, after adjusting for lowest noise only via the small microring resonators, while also mon-

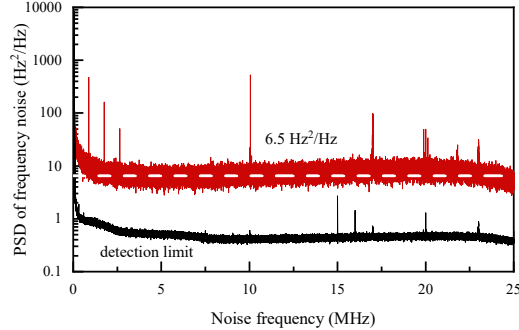


Figure 10: Double-sided power spectral density (PSD) of laser frequency noise for a pump current of 255 mA, plotted for positive frequencies. The dashed line at $6.5 \text{ Hz}^2/\text{Hz}$ represents the mean of PSD values for noise frequencies between 4 and 7.5 MHz. The detection limit is at $0.5 \text{ Hz}^2/\text{Hz}$.

itoring the optical spectrum with an OSA to verify single-mode oscillation. The laser noise spectrum becomes flat towards noise frequencies above $> 2 \text{ MHz}$. The upper bound for the white noise limit, indicated as dashed line, is taken as $6.5 \pm 1.3 \text{ Hz}^2/\text{Hz}$. These values are obtained by taking the mean value and standard deviation of the Gaussian distribution of PSD values between noise frequencies of 4 and 7.5 MHz. After multiplying with 2π this corresponds to an intrinsic linewidth of $40 \pm 8 \text{ Hz}$.

To verify the low linewidth level, the measurement is repeated with the second heterodyne setup using the same heater settings. The pump current was increased and decreased in steps and fine-tuned for lowest RF linewidth, while monitoring the optical spectrum with an OSA for single-mode oscillation. Figure 11 displays the Lorentzian linewidth component vs laser output power expressed as the factor of pump power above threshold, X , where the error bars express the uncertainty in fitting. A doubly logarithmic plot is chosen to facilitate comparison with the expected inverse power law dependence of the linewidth as straight line with negative unity slope. The red line is a least-square fit with fixed negative unity slope vs the inverse threshold factor, $\frac{1}{X}$, showing that the measured linewidth narrows ap-

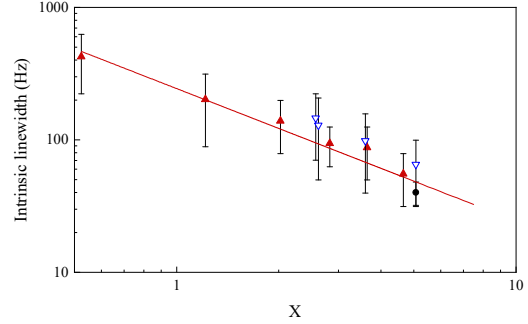


Figure 11: Lorentzian linewidth versus the threshold factor, X , which is proportional to the output power, P_{out} . Unfilled symbols show measurements vs decreasing power. Measurements vs increasing power (filled symbols) yield slightly smaller linewidths. The solid line is a least-square fit to the lower linewidth data with negative unity slope (inverse power law, $\propto P_{\text{out}}^{-1}$). The linewidth obtained from PSD measurements (Fig. 10) is shown as a black round symbol at $X = 5.07$ (255 mA pump current).

proximately inversely with laser power as theoretically expected. The power narrowing data do not display a levelling-off, in spite of significant intensity build-up in the high-finesse ring resonators. The lowest linewidth obtained from power spectral density recordings (shown as round symbol for comparison) is in good agreement with the data obtained from Lorentz fitting. The linewidth limit of 40 Hz in Fig. 10 is the narrowest intrinsic linewidth ever reported for an integrated diode laser.

5 Conclusions

We have demonstrated a hybrid integrated and widely tunable single-frequency diode laser with an intrinsic linewidth as low as 40 Hz , a spectral coverage of more than 70 nm and a maximum fiber-coupled output of 23 mW . The narrow linewidth is achieved via feedback from a low-loss dielectric waveguide circuit that extends the laser cavity to a roundtrip length of 0.5 m , in combination with single-mode resolving filtering. Realizing such high-finesse

filtering with cascaded microring resonators with essentially a single roundtrip through a long and low-loss feedback arm allows strong linewidth narrowing in the presence of significant laser cavity roundtrip losses. The tolerance to loss in this approach is important because semiconductor amplifiers are intrinsically lossy, such as also the mode transitions between different waveguide platforms in hybrid or heterogeneously integrated photonic circuits. Choosing dielectric feedback waveguides based on silicon nitride is important for avoiding nonlinear loss because GW/cm^2 -level intensities readily occur in lasers with tens of mW output and high-finesse intracavity filtering. The approach demonstrated here is promising for further linewidth narrowing through stronger pumping, as no hard linewidth limit through nonlinear loss is apparent with dielectric feedback circuits. Much promise lies also in further extension of the cavity length in combination with tighter filtering. This route appears very feasible because silicon nitride waveguides can be fabricated with extremely low loss down to 0.045 dB/m [47], while several meter long silicon nitride resonator circuits have been demonstrated with a spectral selectivity better than 100 MHz [48]. These properties and options indicate the feasibility of Hertz-level integrated diode lasers on a chip.

Funding Information

This research was funded by the IOP Photonic Devices program of RVO (Rijksdienst voor Onderzoek Nederland), a division of the Ministry for Economic Affairs, The Netherlands and in part by the European Union's Horizon 2020 research and innovation programme under grant agreement 780502 (3PEAT).

Disclosures

The authors declare no conflicts of interest.

References

- [1] D. Marpaung and J. Yao, "Integrated microwave photonics," *Nat. Photonics* **13**, 80–90 (2019).
- [2] L. Zhuang, C. G. H. Roeloffzen, A. Meijerink, M. Burla, D. A. I. Marpaung, A. Leinse, M. Hoekman, R. G. Heideman, and W. van Etten, "Novel ring resonator-based integrated photonic beamformer for broadband phased array receive antennas—part II: Experimental prototype," *J. Light. Technol.* **28**, 19–31 (2010).
- [3] S. Zhang, P. Y. Kam, C. Yu, and J. Chen, "Laser linewidth tolerance of decision-aided maximum likelihood phase estimation in coherent optical M-ary PSK and QAM systems," *IEEE Photonics Technol. Lett.* **21**, 1075–1077 (2009).
- [4] J. E. Koroshetz, "Fiber lasers for lidar," in *Optical Fiber Communication Conference and Exposition and The National Fiber Optic Engineers Conference*, (Optical Society of America, 2005), p. OFJ4.
- [5] L. He, S. Özdemir, J. Zhu, W. Kim, and L. Yang, "Detecting single viruses and nanoparticles using whispering gallery microlasers," *Nat. Nanotechnol.* **6**, 428–432 (2011).
- [6] A. Hemmerich, D. McIntyre, D. Schropp, D. Meschede, and T. Hänsch, "Optically stabilized narrow linewidth semiconductor laser for high resolution spectroscopy," *Opt. Commun.* **75**, 118–122 (1990).
- [7] Y. Jiang, A. Ludlow, N. Lemke, R. Fox, J. Sherman, L.-S. Ma, and C. Oates, "Making optical atomic clocks more stable with 10^{-16} -level laser stabilization," *Nat. Photonics* **5**, 158–161 (2011).
- [8] Z. L. Newman, V. Maurice, T. Drake, J. R. Stone, T. C. Briles, D. T. Spencer, C. Fredrick, Q. Li, D. Westly, B. R. Ilic, B. Shen, M.-G. Suh, K. Y. Yang, C. Johnson, D. M. S. Johnson, L. Hollberg, K. J. Vahala, K. Srinivasan, S. A. Diddams, J. Kitching, S. B. Papp, and

M. T. Hummon, "Architecture for the photonic integration of an optical atomic clock," *Optica* **6**, 680–685 (2019).

[9] S. M. Spillane, T. J. Kippenberg, and K. J. Vahala, "Ultralow-threshold Raman laser using a spherical dielectric microcavity," *Nature* **415**, 621–623 (2002).

[10] J. Li, M.-G. Suh, and K. Vahala, "Microresonator Brillouin gyroscope," *Optica* **4**, 346–348 (2017).

[11] S. Gundavarapu, G. M. Brodnik, M. Puckett, T. Huffman, D. Bose, R. Behunin, J. Wu, T. Qiu, C. Pinho, N. Chauhan, J. Nohava, P. T. Rakich, K. D. Nelson, M. Salit, and D. J. Blumenthal, "Sub-Hertz fundamental linewidth photonic integrated Brillouin laser," *Nat. Photonics* **13**, 60–67 (2019).

[12] B. Stern, X. Ji, Y. Okawachi, A. L. Gaeta, and M. Lipson, "Battery-operated integrated frequency comb generator," *Nature* **562**, 401–405 (2018).

[13] A. S. Raja, A. S. Voloshin, H. Guo, S. E. Agafonova, J. Liu, A. S. Gorodnitskiy, M. Karpov, N. G. Pavlov, E. Lucas, R. R. Galiev, A. E. Shitikov, J. D. Jost, M. L. Gorodetsky, and T. J. Kippenberg, "Electrically pumped photonic integrated soliton microcomb," *Nat. Commun.* **10**, 680 (2019).

[14] A. L. Schawlow and C. H. Townes, "Infrared and optical masers," *Phys. Rev.* **112**, 1940–1949 (1958).

[15] M. Lax, "Classical noise. V. Noise in self-sustained oscillators," *Phys. Rev.* **160**, 290–307 (1967).

[16] Y. A. Akulova, G. A. Fish, P.-C. Koh, C. L. Schow, P. Kozodoy, A. P. Dahl, S. Nakagawa, M. C. Larson, M. P. Mack, T. A. Strand, C. W. Coldren, E. Hegblom, S. K. Penniman, T. Wipiejewski, and L. A. Coldren, "Widely tunable electroabsorption-modulated sampled-grating DBR laser transmitter," *IEEE J. on Sel. Top. Quantum Electron.* **8**, 1349–1357 (2002).

[17] T. Kita, R. Tang, and H. Yamada, "Compact silicon photonic wavelength-tunable laser diode with ultra-wide wavelength tuning range," *Appl. Phys. Lett.* **106**, 111104 (2015).

[18] J. C. Hulme, J. K. Doylend, and J. E. Bowers, "Widely tunable Vernier ring laser on hybrid silicon," *Opt. Express* **21**, 19718–19722 (2013).

[19] N. Kobayashi, K. Sato, M. Namiwaka, K. Yamamoto, S. Watanabe, T. Kita, H. Yamada, and H. Yamazaki, "Silicon photonic hybrid ring-filter external cavity wavelength tunable lasers," *J. Light. Technol.* **33**, 1241–1246 (2015).

[20] M. A. Tran, D. Huang, J. Guo, T. Komljenovic, P. A. Morton, and J. E. Bowers, "Ring-resonator based widely-tunable narrow-linewidth Si/InP integrated lasers," *IEEE J. Sel. Top. Quantum Electron.* **26**, 1500514 (2020).

[21] T. Matsumoto, A. Suzuki, M. Takahashi, S. Watanabe, S. Ishii, K. Suzuki, T. Kaneko, H. Yamazaki, and N. Sakuma, "Narrow spectral linewidth full band tunable laser based on waveguide ring resonators with low power consumption," in *Optical Fiber Communication Conference*, (Optical Society of America, 2010), p. OThQ5.

[22] H. Debregeas, C. Ferrari, M. A. Cappuzzo, F. Klemens, R. Keller, F. Pardo, C. Bolle, C. Xie, and M. P. Earnshaw, "2 kHz linewidth C-band tunable laser by hybrid integration of reflective SOA and SiO₂ PLC external cavity," in *2014 International Semiconductor Laser Conference*, (2014), pp. 50–51.

[23] R. M. Oldenbeuving, E. J. Klein, H. L. Offerhaus, C. J. Lee, H. Song, and K. J. Boller, "25 kHz narrow spectral bandwidth of a wavelength tunable diode laser with a short waveguide-based external cavity," *Laser Phys. Lett.* **10**, 015804 (2013).

[24] Y. Fan, R. M. Oldenbeuving, E. J. Klein, C. J. Lee, H. Song, M. R. H. Khan, H. L. Offerhaus, P. J. M. van der Slot, and K.-J. Boller, “A hybrid semiconductor-glass waveguide laser,” in *Proceedings of SPIE*, , vol. 9135 (2014), p. 91351B.

[25] Y. Fan, R. M. Oldenbeuving, C. G. Roeloffzen, M. Hoekman, D. Geskus, R. G. Heideman, and K.-J. Boller, “290 Hz intrinsic linewidth from an integrated optical chip-based widely tunable InP-Si₃N₄ hybrid laser,” in *Conference on Lasers and Electro-Optics*, (Optical Society of America, 2017), p. JTh5C.9.

[26] C. T. Santis, Y. Vilenchik, N. Satyan, G. Rakuljic, and A. Yariv, “Quantum control of phase fluctuations in semiconductor lasers,” *Proc. Natl. Acad. Sci.* **115**, E7896–E7904 (2018).

[27] D. Huang, M. A. Tran, J. Guo, J. Peters, T. Komljenovic, A. Malik, P. A. Morton, and J. E. Bowers, “High-power sub-kHz linewidth lasers fully integrated on silicon,” *Optica* **6**, 745–752 (2019).

[28] Y. Vilenchik, C. T. Santis, S. T. Steger, N. Satyan, and A. Yariv, “Theory and observation on non-linear effects limiting the coherence properties of high-Q hybrid Si/III-V lasers,” in *Novel in-plane semiconductor lasers XIV*, , vol. 9382 (International Society for Optics and Photonics, 2015), p. 93820N.

[29] B. Kuyken, F. Leo, S. Clemmen, U. Dave, R. Van Laer, T. Ideguchi, H. Zhao, X. Liu, J. Safioui, S. Coen, S. Gorza, S. K. Selvaraja, S. Massar, R. M. Osgood, P. Verheyen, J. Van Campenhout, R. Baets, W. M. J. Green, and G. Roelkens, “Nonlinear optical interactions in silicon waveguides,” *Nanophotonics* **6**, 377–392 (2017).

[30] E. Patzak, A. Sugimura, S. Saito, T. Mukai, and H. Olesen, “Semiconductor laser linewidth in optical feedback configurations,” *Electron. Lett.* **19**, 1026–1027 (1983).

[31] C. Henry, “Theory of spontaneous emission noise in open resonators and its application to lasers and optical amplifiers,” *J. Light. Technol.* **4**, 288–297 (1986).

[32] K. Ujihara, “Phase noise in a laser with output coupling,” *IEEE J. Quantum Electron.* **20**, 814–818 (1984).

[33] G. Bjork and O. Nilsson, “A tool to calculate the linewidth of complicated semiconductor lasers,” *IEEE J. Quantum Electron.* **23**, 1303–1313 (1987).

[34] T. L. Koch and U. Koren, “Semiconductor lasers for coherent optical fiber communications,” *J. Light. Technol.* **8**, 274–293 (1990).

[35] Y. Fan, R. E. M. Lammerink, J. Mak, R. M. Oldenbeuving, P. J. M. van der Slot, and K.-J. Boller, “Spectral linewidth analysis of semiconductor hybrid lasers with feedback from an external waveguide resonator circuit,” *Opt. Express* **25**, 32767–32782 (2017).

[36] C. Henry, “Theory of the linewidth of semiconductor lasers,” *IEEE J. Quantum Electron.* **18**, 259–264 (1982).

[37] R. Kazarinov and C. Henry, “The relation of line narrowing and chirp reduction resulting from the coupling of a semiconductor laser to passive resonator,” *IEEE J. Quantum Electron.* **23**, 1401–1409 (1987).

[38] N. A. Olsson, C. H. Henry, R. F. Kazarinov, H. J. Lee, and B. H. Johnson, “Relation between chirp and linewidth reduction in external Bragg reflector semiconductor lasers,” *Appl. Phys. Lett.* **51**, 92–93 (1987).

[39] C. G. H. Roeloffzen, M. Hoekman, E. J. Klein, L. S. Wevers, R. B. Timens, D. Marchenko, D. Geskus, R. Dekker, A. Alippi, R. Grootjans, A. van Rees, R. M. Oldenbeuving, J. P. Epping, R. G. Heideman, K. Wrhoff, A. Leinse, D. Geuzebroek, E. Schreuder, P. W. L. van Dijk, I. Visscher, C. Taddei, Y. Fan, C. Taballione, Y. Liu, D. Marpaung, L. Zhuang, M. Benelajla, and K. Boller, “Low-loss Si₃N₄ TriPleX optical waveguides: Technology and applications

overview,” IEEE J. Sel. Top. Quantum Electron. **24**, 1–21 (2018).

[40] Y. Fan, J. P. Epping, R. M. Oldenbeuving, C. G. H. Roeloffzen, M. Hoekman, R. Dekker, R. G. Heideman, P. J. M. van der Slot, and K.-J. Boller, “Optically integrated InP-Si₃N₄ hybrid laser,” IEEE Photonics J. **8**, 1–11 (2016).

[41] B. Liu, A. Shakouri, and J. E. Bowers, “Passive microring-resonator-coupled lasers,” Appl. Phys. Lett. **79**, 3561–3563 (2001).

[42] C. J. Krückel, A. Fülop, Z. Ye, P. A. Andrekson, and V. Torres-Company, “Optical bandgap engineering in nonlinear silicon nitride waveguides,” Opt. Express **25**, 15370–15380 (2017).

[43] C. Becher, E. Gehrig, and K.-J. Boller, “Spectrally asymmetric mode correlation and intensity noise in pump-noise-suppressed laser diodes,” Phys. Rev. A **57**, 3952–3960 (1998).

[44] S. Latkowski, A. Hnsel, N. Bhattacharya, T. de Vries, L. Augustin, K. Williams, M. Smit, and E. Bente, “Novel widely tunable monolithically integrated laser source,” IEEE Photonics J. **7**, 1–9 (2015).

[45] L. Richter, H. Mandelberg, M. Kruger, and P. McGrath, “Linewidth determination from self-heterodyne measurements with subcoherence delay times,” IEEE J. Quantum Electron. **22**, 2070–2074 (1986).

[46] L. B. Mercer, “1/f frequency noise effects on self-heterodyne linewidth measurements,” J. Light. Technol. **9**, 485–493 (1991).

[47] J. F. Bauters, M. J. R. Heck, D. D. John, J. S. Barton, C. M. Bruinink, A. Leinse, R. G. Heideman, D. J. Blumenthal, and J. E. Bowers, “Planar waveguides with less than 0.1 dB/m propagation loss fabricated with wafer bonding,” Opt. Express **19**, 24090–24101 (2011).

[48] C. Taddei, L. Zhuang, C. G. H. Roeloffzen, M. Hoekman, and K. Boller, “High-selectivity on-chip optical bandpass filter with sub-100-MHz flat-top and under-2 shape factor,” IEEE Photonics Technol. Lett. **31**, 455–458 (2019).